Tunable meta-atom using liquid metal embedded in stretchable polymer

Peng Liu,[1,a)] Siming Yang,[1,a)] Aditya Jain,[1,2] Qiugu Wang,[1] Huawei Jiang,[1] Jiming Song,[1] Thomas Koschny,[2] Costas M. Soukoulis,[2] and Liang Dong[1,b)]
[1]*Department of Electrical and Computer Engineering, Iowa State University, Ames, Iowa 50011, USA*
[2]*Ames Laboratory, U.S. DOE and Department of Physics and Astronomy, Iowa State University, Ames, Iowa 50011, USA*

(Received 5 May 2015; accepted 25 June 2015; published online 6 July 2015)

Reconfigurable metamaterials have great potential to alleviate complications involved in using passive metamaterials to realize emerging electromagnetic functions, such as dynamical filtering, sensing, and cloaking. This paper presents a new type of tunable meta-atoms in the X-band frequency range (8–12 GHz) toward reconfigurable metamaterials. The meta-atom is made of all flexible materials compliant to the surface of an interaction object. It uses a liquid metal-based split-ring resonator as its core constituent embedded in a highly flexible elastomer. We demonstrate that simple mechanical stretching of the meta-atom can lead to the great flexibility in reconfiguring its resonance frequency continuously over more than 70% of the X-band frequency range. The presented meta-atom technique provides a simple approach to dynamically tune response characteristics of metamaterials over a broad frequency range. © *2015 AIP Publishing LLC*.
[http://dx.doi.org/10.1063/1.4926417]

I. INTRODUCTION

Flexible electronics have gained considerable attention because of their potential applications in artificial skins, flexible displays, wearable sensors, sustainable energy, etc. Many flexible electronic devices have recently been developed, such as stretchable integrated circuits,[1–5] microfluidic antennas,[6–8] three-dimensional energy devices,[9] printed thin film transistors,[10–13] and biomimetic pressure sensors.[14] On the other hand, electromagnetic (EM) metamaterials have been intensively studied because they possess intriguing properties unattainable with naturally existing materials, such as negative permittivity and permeability.[15–27] Split-ring resonator (SRR) is a popular building block of many metamaterial-based resonant devices in the microwave regime.[28–31] But, these resonant devices often have a limited bandwidth. If the response characteristics are dynamically tunable, these resonant devices will become more useful when adapting to different applications. To this end, many tunable metamaterial technologies have been demonstrated, based on changing unit cell's effective circuit parameters,[32–36] constituent material properties,[37–42] or geometries.[43–49] Specifically, the circuit tuning method uses variable capacitors and switches to change individual impedances of unit cells.[32–36] Tuning of the constituent materials relies on using phase change materials or liquid crystal to change properties of materials that make up unit cells.[37–42] The micro-electro-mechanical systems and microfluidics based approaches change structures and locations of unit cells relative to a fixed part of metamaterials.[43–49]

While the existing tunable metamaterial technologies have led to significant improvement toward broadening dynamic tuning ranges of the EM properties of microwave metamaterials, there is still much room for improvement such as simplifying resonance tuning mechanism, extending tuning range, and making metamaterials flexible enough to comply with surface irregularities on the underlying substrate. For example, a switchable metamaterial has recently been developed, capable of tuning its resonance frequency by pumping mercury into and out of SRR-shaped microchannels via a relatively complex microfluidic control system.[41] A tunable liquid metal-based antenna has also been realized by injecting a liquid metal alloy into a microchannel made of a stretchable elastomer.[6] This device could be stretched to more than double of its original length, thus obtaining a wide frequency tuning range.

In this paper, we present a novel stretchable SRR-based meta-atom capable of tuning its EM response characteristics over a broad frequency range via simple mechanical stretching. The presented meta-atom uses a liquid metal as the resonator material. The liquid metal is patterned to be a SRR structure and embedded inside a highly stretchable silicone elastomer. Due to its liquid nature, the SRR can flow in response to applied strains, and thus, is not prone to fatigue or cracking. When the encasing elastomer is stretched and twisted, the SRR will be sufficiently compliant to yield all necessary deformation. Therefore, by changing the shape of the SRR via mechanical stretching, the split gap capacitance and the inductance of the SRR can be adjusted, thus tuning the resonance response of the meta-atom.

II. DESIGN AND FABRICATION

To test the concept of mechanically tunable meta-atom, we designed a liquid metal SRR to operate in the X-band frequency range (Fig. 1). While many types of liquid metal may be used, the SRR in this study employed eutectic gallium-indium or EGaIn (75.5% gallium and 24.5% indium; a liquid

[a)]P. Liu and S. Yang contributed equally to this work.
[b)]Author to whom correspondence should be addressed. Electronic mail: ldong@iastate.edu.

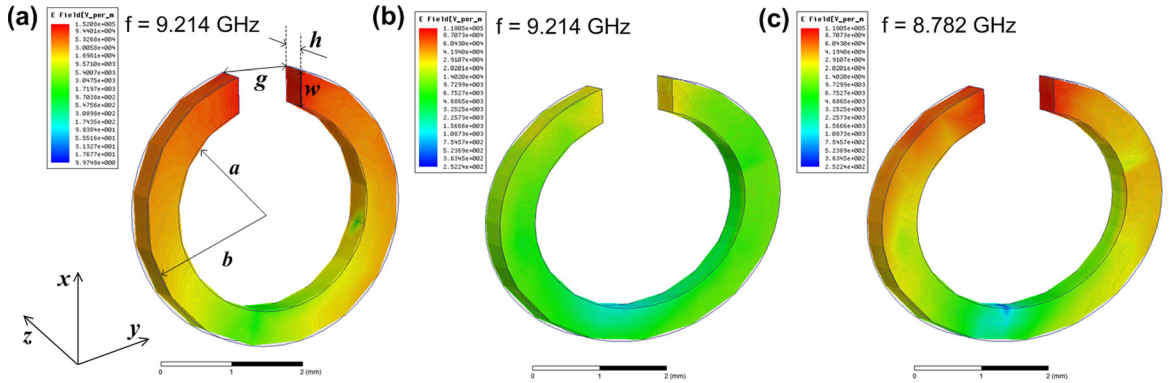

FIG. 1. Simulated magnitude of the electric field (E) distributions in the tunable liquid metal SRR at the resonance frequency of 9.214 GHz when not stretched (a), at 9.214 GHz when stretched by 30% along the *y* direction (b), and at a new resonance frequency of 8.782 GHz at the stretched state (c).

at room temperature and a solid at 14 °C) because of its favorable attributes, such as high electrical conductivity, low toxicity, and light weight. The liquid metal SRR had the inner radius of $a = 1.5$ mm, the outer radius of $b = 2.0$ mm, the thickness of $h = 0.5$ mm, and the gap distance of $g = 1.0$ mm. The SRR was encased by Ecoflex, a highly stretchable silicone elastomer with the maximal elongation at break of 900%. It is noteworthy that Ecoflex is thermally curable and suitable for replica molding from a master mold, just like polydimethylsiloxane, a commonly used elastomer in soft lithography. The length, width, and thickness of the Ecoflex encasing membrane were $l = 11.0$ mm, $d = 7.5$ mm, and $t = 1.45$ mm, respectively.

The resonant response of a SRR can be equivalently regarded as a LC resonator with a resonance frequency of $f_o = 1/(2\pi\sqrt{LC})$, where the inductance L results from the current path of the SRR, and the capacitance C is determined by the split gap and the dielectric properties of the substrate along with the material that fills the gap. In this study, when the SRR was stretched, both of the capacitance and inductance would change, thus shifting the resonance frequency. To illustrate the influence of mechanical stretching on the resonance of the SRR, we conducted EM simulations using the Ansys High Frequency Structure Simulator (HFSS) software. As shown in Fig. 1, the SRR was fixed in the *x*-*y* plane inside a waveguide and the magnetic field (H) was parallel to the *z* direction and penetrated through the SRR, thus exciting the magnetic resonance. When the split gap of the SRR was aligned along the *y* direction, the resonance frequency before stretch was at 9.214 GHz (Fig. 1(a)). Applying the stretch of 30% along the *y* direction led to an increase in the split gap along the same direction (Fig. 1(b)). As a result, the SRR was brought out of resonance at 9.214 GHz and resonated at a new frequency of 8.782 GHz (Fig. 1(c)). We note that the simulation here only conceptually illustrated the proposed tuning mechanism. The more quantitative simulation results are presented and discussed later, together with the experimental results.

Figure 2 shows the fabrication process flow for the tunable meta-atom. First, to form the SRR-shaped microchannels, an 800-μm-thick Ecoflex layer L1 was cast upon a master mold made of SU-8 photoresist on a silicon (Si) wafer W1, and then, was fully cured at 60 °C on a hotplate for 30 min (Figs. 2(a) and 2(b)). In a parallel process, a 100-μm-thick Ecoflex thin layer L2 was spin-coated on another Si wafer W2, followed by partial curing at 50 °C on a hotplate for 40 s (Fig. 2(c)). Subsequently, the layer L1 was peeled off from the master mold and adhered to the partially cured layer L2. The two layers L1 and L2 were then permanently and thermally bonded together on a hotplate at 90 °C for 30 min (Fig. 2(d)). After the two bonded layers were peeled off from the wafer W2, the liquid metal EGaIn was injected into the embedded microchannels through two 100-μm-diameter holes mechanically punched at the two ends of each microchannel. There were some residues of the eutectic alloy remaining around the holes on the top surface of the Ecoflex structure. To clean the top surface, a cotton swab was dipped

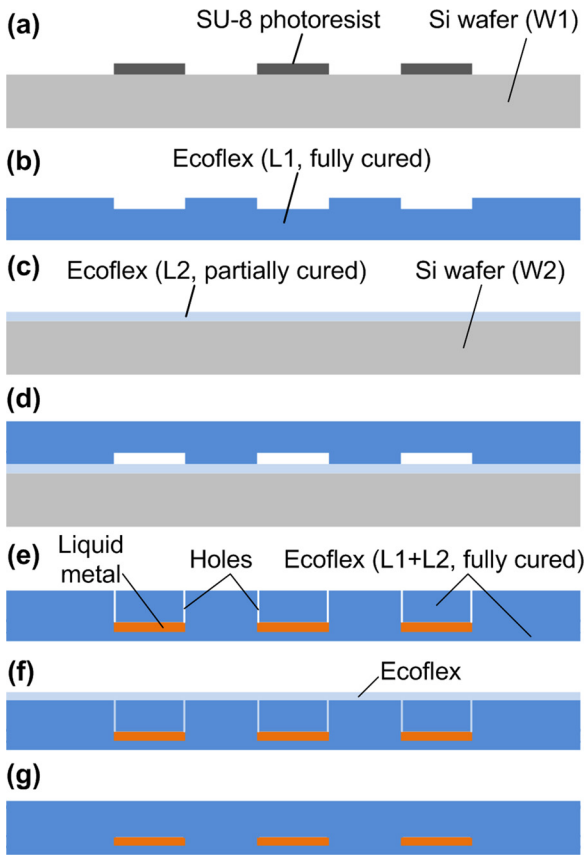

FIG. 2. Fabrication process for the tunable liquid metal SRR.

in a solution of hydrochloric acid (50%, v/v) and then carefully wiped off any residues from the top surface (Fig. 2(e)). To encapsulate the liquid metal inside the Ecoflex elastomer, a new Ecoflex prepolymer solution was poured onto the cleaned top surface, followed by a full curing process performed at 80 °C on a hotplate for 30 min (Figs. 2(f) and 2(g)). Therefore, the liquid metal SRRs were formed inside the elastomer. The total thickness of the elastomer was 1.45 mm as mentioned. The SRRs were located nearly at half the thickness of the elastomer. Lastly, individual SRRs were diced out of the whole elastomer for testing.

III. EM MEASUREMENT CONFIGURATIONS

After the meta-atom was formed, we carried out the EM measurements over the X-band using a WR90 rectangular waveguide (22.86×10.16 mm) terminated by a UG39/U cover flange. When the waves propagated in the waveguide, the directions of E and H were along the short edge and the long edge of the waveguide, respectively. The walls of the waveguide acted as reflective mirrors and made the SRR cell behave as an element in a 2D quasi-periodic structure with normal incidence wave. The SRR sample was attached onto a wood slab (low-loss microwave substrate material) and centered in the middle of the waveguide. Multiple cotton wires were inserted through the holes prepunched at the opposite ends of the Exoflex elastomer. The elastomer was then stretched to a specified strain level (17%, 28%, 53%, or 72%). To hold the sample in place, the cotton wires passed through the holes predrilled in the wood slab and then rolled and tied on the wood posts at the backside of the slab. The spectra were measured using a programmable vector network analyzer (Agilent E8364). A full 2-port calibration was performed to set an accurate reference plane before the measurement.

There were six possible arrangements for the SRR inside the waveguide, as illustrated in Fig. 3. But only three of them (Figs. 3(a), 3(c), and 3(d)) were able to excite the resonance of the circular ring current in the SRR (magnetic dipole resonance). Figure 3(a) displays that the incident wave was normal to the plane of the ring and the E field was parallel to the gap direction. The electric dipole formed across the split gap allowed coupling of the E field of the waveguide mode to the magnetic dipole resonance of the SRR because of the broken symmetry of the ring with respect to the E-field direction. In the case shown in Fig. 3(c), both the electric moment across the gap driven by the incident E field and the magnetic moment of the circular ring induced by the incident H field current jointly excite the resonance of the ring. Figure 3(d) shows that the H field is normal to the plane of the ring, which induces the circulating current in the ring and generate magnetic moment. Neither electric nor magnetic dipole moment could couple to the incident waveguide mode in the other three configurations shown in Figs. 3(b), 3(e), and 3(f).

IV. RESULTS AND DISCUSSION

In the first measurement configuration (Fig. 3(a)), the SRR was stretched along the H-field direction with different

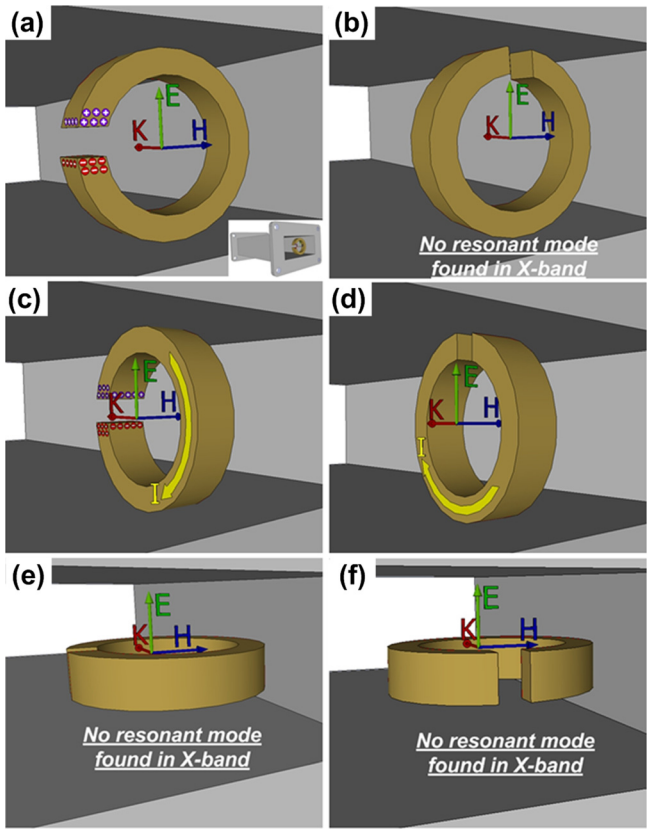

FIG. 3. Six possible configurations of the SRR inside a testing waveguide. The inset in (a) shows the relative location of the ring to the waveguide. The electric dipole formed by opposite electric charges accumulating across the gap of the ring couples the SRR resonance to the E field of the incident waveguide mode in (a) and (c). The magnetic dipole moment due to the loop current couples to the incident H field normal to the ring plane in (c) and (d). No coupling to the resonance was found in (b), (e), and (f) in X-band.

stretch ratios. The E field was formed across the split gap to excite the electric resonance that corresponded to a transmission dip at the resonance frequency in the transmittance spectrum (see supplementary Fig. S1 for the reflectance spectrum[50]). The experimental result in Fig. 4(a) shows that by stretching the SRR, the resonance was progressively tuned to the lower frequencies. For the stretch ratio of 17%, 28%, 53%, and 72%, the resonance frequency red shifted from 10.54 GHz to 9.78 GHz, 9.05 GHz, 8.52 GHz, and 7.67 GHz, respectively. The deformation of the SRR under different stretch levels was observed to be consistent with the simulated deformation using the finite element method analysis (FEA) with the COMSOL Multiphysics (Fig. 4(b)). The embedded liquid metal was also found to remain continuous while being compliant to the changing shape of the surrounding elastomer.

We modeled the SRR and conducted simulations for its resonance response to different stretching magnitudes using the full-wave 3D EM simulation tool in the CST Studio. The surface geometric parameters of the deformed SRR and elastomer structures were extracted from their top-view images. The thicknesses of the liquid metal and the elastomer were estimated by dividing their respective volume by the corresponding surface area. In this simulation, the SRR was placed in a rectangular waveguide with four metal walls, the

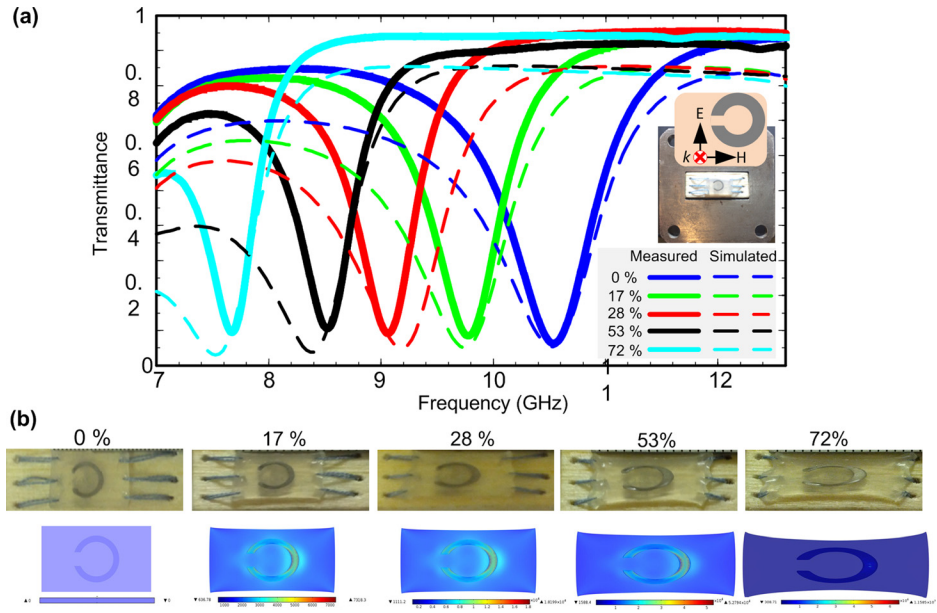

FIG. 4. (a) Measured and simulated transmittance spectra of the tunable liquid metal SRR meta-atom at different stretching ratios of 0, 17%, 28%, 53%, and 72%, when the meta-atom was placed inside the waveguide as shown in the inset. Also, refer to Fig. 3(a) for the measurement arrangement. The conductivity of liquid metal was 3.46×10^6 S/m. The dielectric constant and loss tangent of Ecoflex silicone rubber was 2.5 and 0.01, respectively. The SRR was placed on a wood substrate with the dielectric constant of 1.22 and the loss tangent of 0.1. (b) Experimental (left) and corresponding simulated (right) results for the stretch-induced mechanical deformations of the tunable meta-atom.

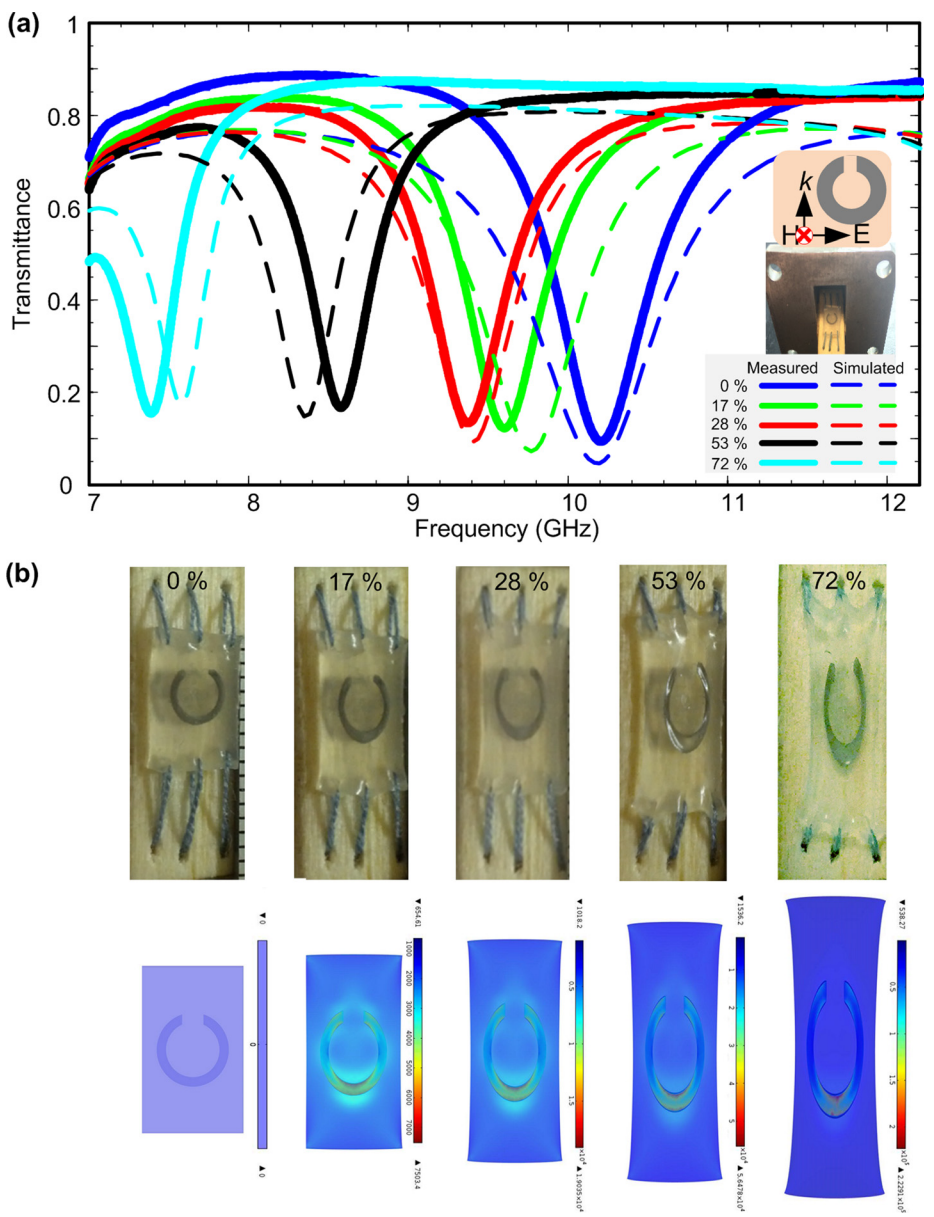

FIG. 5. (a) Measured and simulated transmittance spectra of the tunable liquid metal SRR meta-atom at different stretching ratios of 0, 17%, 28%, 53%, and 72%, when the meta-atom was placed inside the waveguide as shown in the inset. Also, refer to Fig. 3(c) for the measurement arrangement. (b) Experimental (upper) and corresponding simulated (lower panel) results for the stretch-induced mechanical deformations of the tunable meta-atom.

same as the experimental measurement setup. The simulated transmittance spectra of the SRR were presented with dotted lines along with the experimental result in Fig. 4(a).

In the second measurement configuration (Fig. 3(c)), the resonance was excited by both of the E and H fields. At the stretch level of 17%, 28%, 53%, and 72%, the resonance frequency was observed to red shift from 10.21 GHz to 9.58 GHz, 9.37 GHz, 8.58 GHz, and 7.37 GHz, respectively (Fig. 5(a)). In the third measurement configuration (Fig. 3(d)), the resonance was induced by the circulating current in the ring caused by the H field. The measurement result shows that at the stretch level of 17%, 28%, 53%, and 72%, the resonance frequency also red shifted from 9.58 GHz to 9.24 GHz, 8.79 GHz, 8.32 GHz, and 7.32 GHz, respectively (Fig. 6(a)). Similarly, Figs. 5(b) and 6(b) show the experimental and simulated geometric changes of the SRR at different stretching levels in the second and third configuration, respectively (see supplementary Figs. S2 and S3 for the reflectance spectrum of the second and the third measurement configuration, respectively[50]).

For all three of the aforementioned configurations, the experimental EM measurement results show good agreement with the simulated results. The slight discrepancy between the simulated and testing results indicates that the 3D model used in the CST-based EM simulation is acceptable. It is also noted that the modeling accuracy mainly depends on the accuracy of the extracted surface geometric parameters and the estimated thickness of the deformed SRR and Ecoflex structures (Figs. 4(b), 5(b), and 6(b)). Nevertheless, as demonstrated, when the same stretch of 72% was applied to the SRR in all the three measurement configurations, the resonance frequency of the SRR was tuned by a net shift of 2.87 GHz (Fig. 4(a)), 2.83 GHz (Fig. 5(a)), and 2.26 GHz (Fig. 6(a)), or a relative shift of 27.2%, 27.8%, and 23.5%, with respect to the original resonance frequency of 10.54 GHz, 10.20 GHz, and 9.58 GHz, respectively. Figure 7 summarizes the relationships between the stretch ratio and the resulting resonance frequency shift.

Although the obtained experimental and CST-based simulation results have demonstrated the ability to tune the resonance frequency of the SRR via mechanical stretching, it is worthwhile to further understand how the equivalent capacitance and inductance of the SRR were influenced by their geometric deformation. The equivalent capacitance is dominated by the split gap capacitance C_{gap}, which is a function of the gap geometry (see Eq. (S1) in supplementary

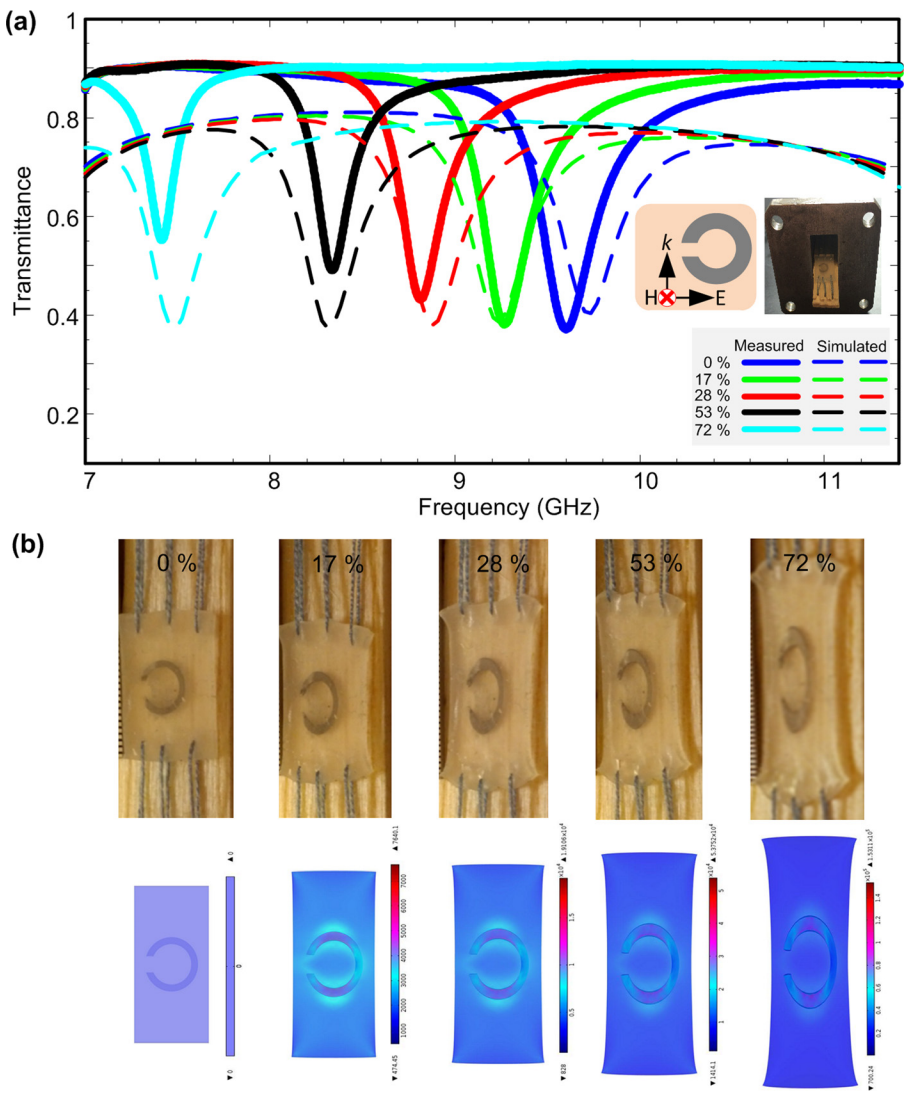

FIG. 6. (a) Measured and simulated transmittance spectra of the tunable liquid metal SRR meta-atom at different stretching ratios of 0, 17%, 28%, 53%, and 72%, when the meta-atom was placed inside the waveguide as shown in the inset. Also, refer to Fig. 3(d) for the measurement arrangement. (b) Experimental (upper) and corresponding simulated (lower panel) results for the stretch-induced mechanical deformations of the tunable meta-atom.

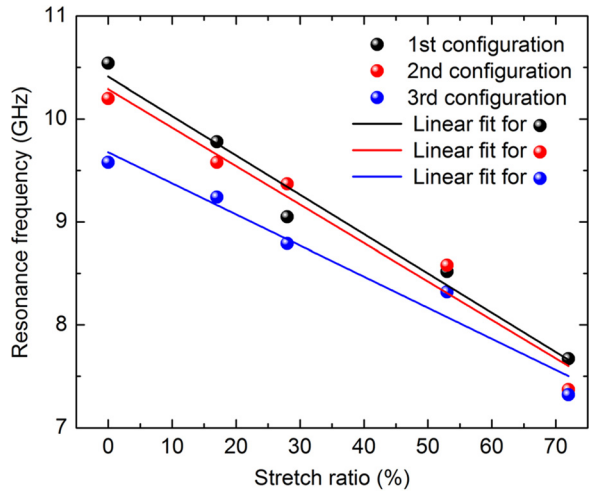

FIG. 7. Resonance frequency as a function of the stretch ratio for the tunable meta-atom in the three measurement configurations shown in Figs. 4–6.

material for the closed-form equation[50]). The equivalent inductance consists of self-inductance of the conducting loop and the mutual inductance induced by the boundary conditions of a given waveguide that are imposed on the SRR for certain orientations (quasi-periodic structure). The self-inductance of an unstretched circular loop L_0 and a stretched elliptical loop L_e are geometrically dependent (see Eqs. (S2) and (S3) in supplementary material for the closed-form equation[50]). The mutual inductance depends not only on the self-inductance but also on the SRR orientations with different mirror effects imposed by the waveguide. We note that in the previous experiments, the resonance modes of the SRR were excited inside a waveguide where mutual interactions with the inner walls of the waveguide existed. But, to simplify the simulation while still illustrating a changing trend of resonance frequency shift, the effect of the mutual interaction into the free-space simulation was excluded, because compared with the effect from the mutual interaction with the walls, the geometric deformation of the SRR could be considered to contribute most to the resonance frequency change. Therefore, we performed EM simulations for a single SRR using HFSS in the free space. Specifically, a delta-gap source was set along the gap direction to excite the unit cell (Fig. 8(a)), and the impedance was monitored while sweeping the frequency. To describe the resonance behavior of the stretching SRR, we designed a one-port equivalent circuit taking into account the equivalent inductance L and capacitance C, the dielectric loss R_d from the substrate, and the metallic loss R_m from the liquid metal (Fig. 8(b)). The lumped L and C were obtained by optimizing the impedance of the equivalent circuit based on the simulated impedance around the resonant frequency with less than 3% of relative error for each stretching case.

The simulation results (Figs. 8(c) and 8(d)) show that as the unit cell was stretched perpendicular to (the first and the second configurations in Figs. 4 and 5) or along (the third configuration in Fig. 6) the gap direction, the equivalent capacitance and inductance increased with increasing the stretch ratio. Since the mechanical stretching in any one of the configurations increased the perimeter of the SRR loop, it is obvious that the inductance would increase with stretching. As for the capacitance, in the first and the second configurations, the stretching caused to decrease the distance between the two arms of the SRR, and also caused to increase the effective metal area that allowed holding more charges. Therefore, the equivalent capacitance of the SRR in these two configurations was increased as increasing the stretch ratio. In the third configuration, despite that the distance between the arms was increased, the stretching also increased the area of liquid metal in the arms region near the split. By further considering the fringing effect, the ability of the SRR to store charges was actually enhanced, thus increasing the equivalent capacitance as well. The simulation result also indicates that the perpendicular stretching (Fig. 8(d)) was more effective than the parallel stretching (Fig.

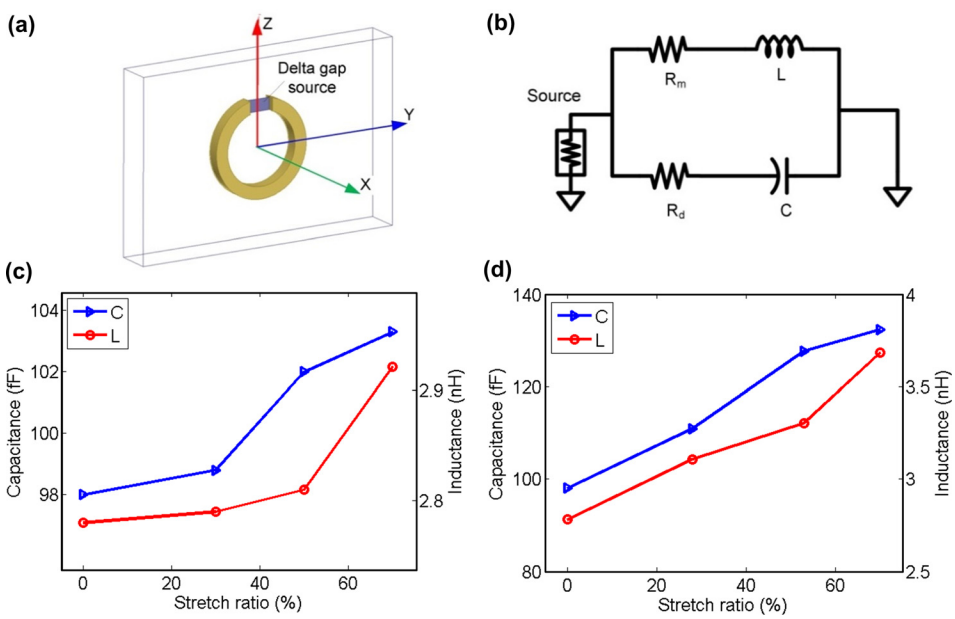

FIG. 8. (a) Schematic of the tunable SRR in the free space. A delta-gap source was set along the split gap. (b) Equivalent circuit of the SRR shown in (a). (c) Simulated capacitance and inductance as a function of the stretch ratio when the SRR was stretched perpendicular to the split gap direction. (d) Simulated capacitance and inductance as a function of the stretch ratio when the SRR was stretched along the gap direction.

8(c)). This is because when the SRR was stretched in the perpendicular direction, the gap distance rapidly decreased to make the delta-gap source more effective.

The present meta-atom exhibited good repeatability in the resonance modulation, as demonstrated with 500 stretching response tests. For each test, the meta-atom was stretched to a same strain level outside the waveguide and then placed back into the waveguide for EM measurement. We note that further elongation of the SRR beyond 72% would move the resonance frequency to below the cutoff frequency of the waveguide used in this study. Nevertheless, even with the applied moderate stretch amplitude, this tunable meta-atom method provided a considerable frequency tuning range covering 71.75% (2.87 GHz divided by 4.0 GHz) of the whole X-band frequency range (8.0–12.0 GHz). Furthermore, by changing its overall size and geometric parameters of the SRR, the original resonance frequency of the SRR can be set to be at the upper limit of the X-band frequency range. By doing that, tuning in the whole X-band frequency range may be achieved with sufficient stretching. Our experiments showed that the present SRR could be stretched by more than twice (>200%) the original size in any directions, while keeping the embedded liquid metal structure continuous, flexible, and recoverable, without breaking of the encasing polymer layer or occurring of structural hysteresis.

V. CONCLUSION

A liquid metal SRR-based tunable meta-atom was demonstrated in the X-band frequency range. The meta-atom consisted of a liquid metal resonator encased by a flexible elastomer skin. By stretching the meta-atom, the resonance frequency of the meta-atom was tuned continuously over more than 70% of the whole X-band frequency range. The meta-atom in this study presents a simple but effective building block for realizing mechanically tunable metamaterials. Also, since the constituent materials of the present meta-atom are relatively ecofriendly, reusable, and durable, the metamaterials made of such meta-atoms potential will find many applications in wearable EM coatings and devices.

ACKNOWLEDGMENTS

The work was partially supported by the National Science Foundation under the Grant No. ECCS-0954765, the Iowa Department of Transportation, the Iowa Highway Research Board, and the China Scholarship Council. The work at Ames Laboratory was partially supported by the U.S. Department of Energy, Office of Basic Energy Science, Division of Materials Sciences and Engineering. Ames Laboratory is operated for the U.S. Department of Energy by Iowa State University under Contract No. DE-AC02-07CH11358.

[1]D.-H. Kim, J.-H. Ahn, W. M. Choi, H.-S. Kim, T.-H. Kim, J. Song, Y. Y. Huang, Z. Liu, C. Lu, and J. A. Rogers, Science **320**, 507 (2008).
[2]D.-H. Kim, Z. Liu, Y.-S. Kim, J. Wu, J. Song, H.-S. Kim, Y. Huang, K.-c. Hwang, Y. Zhang, and J. A. Rogers, Small **5**, 2841 (2009).
[3]J.-H. Ahn, H.-S. Kim, K. J. Lee, S. Jeon, S. J. Kang, Y. Sun, R. G. Nuzzo, and J. A. Rogers, Science **314**, 1754 (2006).
[4]Y. Sun and J. A. Rogers, Adv. Mater. **19**, 1897 (2007).
[5]J. Yoon, S. Y. Hong, Y. Lim, S.-J. Lee, G. Zi, and J. S. Ha, Adv. Mater. **26**, 6580 (2014).
[6]M. Kubo, X. Li, C. Kim, M. Hashimoto, B. J. Wiley, D. Ham, and G. M. Whitesides, Adv. Mater. **22**, 2749 (2010).
[7]J.-H. So, J. Thelen, A. Qusba, G. J. Hayes, G. Lazzi, and M. D. Dickey, Adv. Funct. Mater. **19**, 3632 (2009).
[8]M. R. Khan, G. J. Hayes, J.-H. So, G. Lazzi, and M. D. Dickey, Appl. Phys. Lett. **99**, 013501 (2011).
[9]Y. Yang, G. Ruan, C. Xiang, G. Wang, and J. M. Tour, J. Am. Chem. Soc. **136**, 6187 (2014).
[10]A. C. Arias, S. E. Ready, R. Lujan, W. S. Wong, K. E. Paul, A. Salleo, M. L. Chabinyc, R. Apte, R. A. Street, Y. Wu, P. Liu, and B. Ong, Appl. Phys. Lett. **85**, 3304 (2004).
[11]K. Hong, S. H. Kim, K. H. Lee, and C. D. Frisbie, Adv. Mater. **25**, 3413 (2013).
[12]A. Pierre, M. Sadeghi, M. M. Payne, A. Facchetti, J. E. Anthony, and A. C. Arias, Adv. Mater. **26**, 5722 (2014).
[13]A. d. l., F. Vornbrock, D. Sung, H. Kang, R. Kitsomboonloha, and V. Subramanian, Org. Electron. **11**, 2037 (2010).
[14]W. Wu, X. Wen, and Z. L. Wang, Science **340**, 952 (2013).
[15]H.-T. Chen, J. F. O'Hara, A. K. Azad, A. J. Taylor, R. D. Averitt, D. B. Shrekenhamer, and W. J. Padilla, Nat. Photonics **2**, 295 (2008).
[16]H.-T. Chen, W. J. Padilla, J. M. O. Zide, A. C. Gossard, A. J. Taylor, and R. D. Averitt, Nature **444**, 597 (2006).
[17]A. Jain, P. Tassin, T. Koschny, and C. M. Soukoulis, Phys. Rev. Lett. **112**, 117403 (2014).
[18]D. R. Smith, D. C. Vier, T. Koschny, and C. M. Soukoulis, Phys. Rev. E **71**, 036617 (2005).
[19]D. Schurig, J. J. Mock, B. J. Justice, S. A. Cummer, J. B. Pendry, A. F. Starr, and D. R. Smith, Science **314**, 977 (2006).
[20]D. Shin, Y. Urzhumov, Y. Jung, G. Kang, S. Baek, M. Choi, H. Park, K. Kim, and D. R. Smith, Nat. Commun. **3**, 1213 (2012).
[21]W. Cai, U. K. Chettiar, A. V. Kildishev, and V. M. Shalaev, Nat. Photonics **1**, 224 (2007).
[22]J. Hao, J. Wang, X. Liu, W. J. Padilla, L. Zhou, and M. Qiu, Appl. Phys. Lett. **96**, 251104 (2010).
[23]N. I. Landy, S. Sajuyigbe, J. J. Mock, D. R. Smith, and W. J. Padilla, Phys. Rev. Lett. **100**, 207402 (2008).
[24]J. B. Pendry, D. Schurig, and D. R. Smith, Science **312**, 1780 (2006).
[25]I. M. Pryce, Y. A. Kelaita, K. Aydin, and H. A. Atwater, ACS Nano **5**, 8167 (2011).
[26]X. Zhang and Z. Liu, Nat. Mater. **7**, 435 (2008).
[27]Q. Zhou, Y. Shi, A. Wang, L. Li, D. Zhao, J. Liu, H. Sun, and C. Zhang, J. Opt. **13**, 125102 (2011).
[28]R. A. Shelby, D. R. Smith, and S. Schultz, Science **292**, 77 (2001).
[29]D. R. Smith, W. J. Padilla, D. C. Vier, S. C. Nemat-Nasser, and S. Schultz, Phys. Rev. Lett. **84**, 4184 (2000).
[30]A. A. Zharov, I. V. Shadrivov, and Y. S. Kivshar, Phys. Rev. Lett. **91**, 37401 (2003).
[31]N. Katsarakis, T. Koschny, M. Kafesaki, E. N. Economou, and C. M. Soukoulis, Appl. Phys. Lett. **84**, 2943 (2004).
[32]K. Aydin and E. Ozbay, J. Appl. Phys. **101**, 024911 (2007).
[33]I. Gil, J. Bonache, J. Garcia-Garcia, and F. Martin, IEEE Trans. Microwave Theory Tech. **54**, 2665 (2006).
[34]D. Wang, L. Ran, H. Chen, M. Mu, J. A. Kong, and B.-I. Wu, Appl. Phys. Lett. **91**, 164101 (2007).
[35]J. Han, A. Lakhtakia, and C.-W. Qiu, Opt. Express **16**, 14390 (2008).
[36]G. He, R.-x. Wu, Y. Poo, and P. Chen, J. Appl. Phys. **107**, 093522 (2010).
[37]Y. Poo, R.-x. Wu, G.-h. He, P. Chen, J. Xu, and R.-f. Chen, Appl. Phys. Lett. **96**, 161902 (2010).
[38]R. Pratibha, K. Park, I. I. Smalyukh, and W. Park, Opt. Express **17**, 19459 (2009).
[39]D. H. Werner, D.-H. Kwon, and I.-C. Khoo, Opt. Express **15**, 3342 (2007).
[40]Q. Zhao, L. Kang, B. Du, B. Li, J. Zhou, H. Tang, X. Liang, and B. Zhang, Appl. Phys. Lett. **90**, 011112 (2007).
[41]T. S. Kasirga, Y. N. Ertas, and M. Bayindir, Appl. Phys. Lett. **95**, 214102 (2009).
[42]F. Zhang, Q. Zhao, L. Kang, D. P. Gaillot, X. Zhao, J. Zhou, and D. Lippens, Appl. Phys. Lett. **92**, 193104 (2008).
[43]Y. H. Fu, A. Q. Liu, W. M. Zhu, X. M. Zhang, D. P. Tsai, J. B. Zhang, T. Mei, J. F. Tao, H. C. Guo, X. H. Zhang, J. H. Teng, N. I. Zheludev, G. Q. Lo, and D. L. Kwong, Adv. Funct. Mater. **21**, 3589 (2011).
[44]M. Lapine, D. Powell, M. Gorkunov, I. Shadrivov, R. Marques, and Y. Kivshar, Appl. Phys. Lett. **95**, 084105 (2009).

[45]M. Lapine, I. V. Shadrivov, D. A. Powell, and Y. S. Kivshar, Nat. Mater. **11**, 30 (2012).
[46]W. M. Zhu, A. Q. Liu, X. M. Zhang, D. P. Tsai, T. Bourouina, J. H. Teng, X. H. Zhang, H. C. Guo, H. Tanoto, T. Mei, G. Q. Lo, and D. L. Kwong, Adv. Mater. **23**, 1792 (2011).
[47]D. Bouyge, A. Crunteanu, M. Duran-Sindreu, A. Pothier, P. Blondy, J. Bonache, J. C. Orlianges, and F. Martin, J. Opt. **14**, 114001 (2012).
[48]H. Tao, A. C. Strikwerda, K. Fan, W. J. Padilla, X. Zhang, and R. D. Averitt, J. Infrared, Millimeter, Terahertz Waves **32**, 580 (2011).
[49]W. M. Zhu, W. Zhang, R. F. Huang, S. K. Ting, G. Q. Lo, D. L. Kwong, and A. Q. Liu, in *Proceedings of IEEE MEMS, Taipei*, Taiwan (2013), p. 725.
[50]See supplementary material at http://dx.doi.org/10.1063/1.4926417 for the measured reflectance and transmittance spectra of the meta-atom and the equations used to build an equivalent circuit of the meta-atom.